Co-fibrillization of pathogenic and functional amyloid proteins with gold nanoparticles against amyloidogenesis

Ibrahim Javed[†], Yunxiang Sun[§,#], Jozef Adamcik[‡,#], Bo Wang[§], Aleksandr Kakinen[†], Emily H. Pilkington[†], Feng Ding[§,*], Raffaele Mezzenga[‡], Thomas P. Davis[†,¶,*], and Pu Chun Ke[†,*]

[†]ARC Centre of Excellence in Convergent Bio-Nano Science and Technology, Monash Institute of Pharmaceutical Sciences, Monash University, 381 Royal Parade, Parkville, VIC 3052, Australia [§]Department of Physics and Astronomy, Clemson University, Clemson, SC 29634, USA [‡]Food & Soft Materials, Department of Health Science & Technology, ETH Zurich, Schmelzbergstrasse 9, LFO, E23, 8092, Zurich, Switzerland [¶]Department of Chemistry, University of Warwick, Gibbet Hill, Coventry, CV4 7AL, United Kingdom

Abstract

Biomimetic nanocomposites and scaffolds hold the key to a wide range of biomedical applications. Here we show, for the first time, a facile scheme of co-fibrillizing pathogenic and functional amyloid fibrils via gold nanoparticles (AuNPs) and their applications against amyloidogenesis. This scheme was realized by β-sheet stacking between human islet amyloid polypeptide (IAPP) and the β-lactoglobulin 'corona' of the AuNPs, as revealed by transmission electron microscopy, 3D atomic force microscopy, circular dichroism spectroscopy and molecular dynamics simulations. The biomimetic AuNPs eliminated IAPP toxicity, enabled X-ray destruction of IAPP amyloids, and allowed dark-field imaging of pathogenic amyloids and their immunogenic response by human T cells. In addition to providing a viable new nanotechnology against amyloidogenesis, this study has implications for understanding the *in vivo* cross-talk between amyloid proteins of different pathologies.
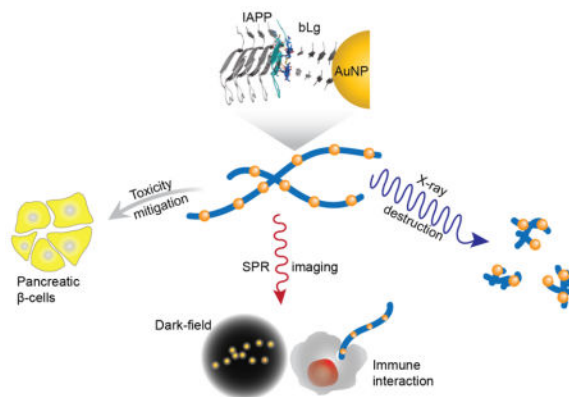
Graphical Abstract

Co-fibrillization of IAPP with bLg-coated AuNPs against amyloidogenesis.

[*]Corresponding Author: Thomas Davis: thomas.p.davis@monash.edu, Feng Ding: fding@clemson.edu and Pu Chun Ke: pu-chun.ke@monash.edu.
[#]YS and JA contributed equally to this work.

Keywords

Amyloidogenesis; protein aggregation; inhibition; gold nanoparticles

INTRODUCTION

The aggregation of proteins and peptides into cross-beta fibrils is a ubiquitous phenomenon associated with neurodegenerative disorders and type 2 diabetes, the amyloid diseases debilitating more than 5% of the global population.[1, 2] Although much progress has been made in the past decades towards understanding the molecular and mesoscopic structures of protein fibrils as well as their fibrillization kinetics and toxicity, there is a crucial lack of strategies for probing the aggregation of amyloid proteins *in situ*, despite their relevance to elucidating the pathologies of amyloid diseases and to the development of effective theranostics.[1, 3]

Nanoparticles (NPs) of metals, semiconductors and oxides possess distinct optical, electrical, magnetic and catalytic properties. The small size of NPs also enables their cellular translocation, biocirculation, and drug delivery. Accordingly, designing biomimetic nanocomposites and scaffolds holds great promise for bioremediation, diagnosis and disease intervention. Recently, Moore et al. examined the effects of gold NPs (AuNPs) on Alzheimer's disease amyloid-β protein aggregation, and found that both the NP size and surface chemistry modulated the extent of protein aggregation while the NP charge influenced the aggregate morphology.[4] Gladytz et al. succeeded in interfacing AuNPs and amyloid proteins,[5] revealing that the amyloid aggregation of human islet amyloid polypeptide (IAPP) and prion protein SUP35 hinged on a balance between peptide-NP and peptide-peptide interactions. Hamley et al. demonstrated labelling of (Ala)10-(His)6 amyloid fibrils with AuNPs.[6] Collectively, these studies demonstrated the feasibility of exploiting NP-protein interactions against amyloidogenesis, an emerging field at the frontiers of materials, medicine, physical sciences, and bioengineering.

IAPP is a 37-residue peptide involved in glycemic control, but its aggregation into amyloids and plaques is a hallmark of type 2 diabetes, a metabolic disease and a global epidemic. In contrast, β-lactoglobulin (bLg) is a natural whey protein which hydrolyzes into small

peptide fragments upon heating and acid exposure (pH 2), and subsequently self-assembles into functional bLg amyloid fibrils.[7, 8] Efficient *in vitro* iron delivery and wastewater purification have been recently demonstrated using bLg amyloids,[9, 10] pointing to the untapped potential of this biomaterial.

To develop biomimetic NPs against amyloidogenesis, we synthesized AuNPs using sonicated bLg amyloids as a β-sheet rich template (bLg AuNPs, ~8 nm in diameter; Scheme and Figure 1), which were then co-fibrillized with pathogenic IAPP. In addition, we synthesized AuNPs stabilized by heat-denatured bLg monomers (bLg-HDM AuNPs, ~6 nm in diameter; Scheme and Figure 1), which had a low β-sheet content. The use of AuNPs in this study was motivated by their biocompatibility as well as their potential for drug delivery, biosensing and photothermal therapy.[11, 12] Following the synthesis, we examined the AuNPs within the context of IAPP fibrillization, toxicity, dark-field imaging, and destruction by localized heating of the AuNPs using X rays. Collectively, our results implicated bLg-AuNPs as a new nanomedicine against amyloidogenesis.

EXPERIMENTAL METHODS

Synthesis of gold nanoparticles (AuNPs)

bLg amyloids were formed according to our reported method.[13] Probe sonicated bLg amyloids (5 mL, 1 mg/mL) were introduced into the refluxing solution (10 mL) of $HAuCl_4$ (0.5 mM) and 200 μL of $NaBH_4$ (0.2 M) was added into the mixture, 30 min later. Heating was stopped after ruby red-colored AuNPs were synthesized and kept on overnight stirring. bLg-HDM AuNPs were synthesized following the same method as with the bLg amyloid fragments. The bLg capped AuNPs were purified via centrifugal filtration. The concentrations of the AuNPs were derived according to the literature.[14]

Synthesis of AuNP-IAPP hybrids

Human islet amyloid polypeptide (IAPP; 37 residues, 2–7 disulfide bridge, 3.9 kDa, >95% pure by HPLC) was obtained in lyophilized monomeric form from AnaSpec, and prepared in Milli-Q water at a stock concentration of 200 μM at room temperature with mixing immediately prior to use. AuNPs were co-fibrillated with IAPP by incubating different concentrations of the NPs with 25 μM of the peptide under ambient conditions for 24 h. bLg AuNPs (0.083 mM) were also incubated with 25 μM Amyloid β (1–42) obtained from AnaSpec, for 72 h in Mili-Q water before TEM visualization.

Transmission electron microscopy and energy-dispersive X-ray spectroscopy

Transmission electron microscopy (TEM) and EDX spectral mapping were performed on an FEI Tecnai F20 transmission electron microscope, operated at 200 kV with the samples adsorbed on a glow discharged (15 s) 400 mesh formvar-coated copper grid. Samples (25 μM of IAPP, 0.083 mM or 0.11 mM of AuNPs) were then stained with 1 % uranyl acetate for visualization.

Dynamic light scattering

Zeta potential and hydrodynamic size were acquired for the two types of AuNPs in aqueous solution (0.1 mM) at room temperature (Malvern Zetasizer). The stability of the AuNPs was evaluated by incubating the AuNPs (0.5 mM) with different concentrations of NaCl at 37 °C for 4 h and then analyzed for aggregation (Table S2).

Circular dichroism spectroscopy

Circular dichroism (CD) spectra of the two types of AuNPs (0.25 mM) were obtained for the wavelength range of 190–240 nm with a 0.5 nm step size at room temperature. The data was converted from mean residue ellipticity (θ) to deg·cm2.dmol-1 and the protein secondary structure was estimated by DichroWeb, using Contin as reference program and reference set4.[15] In addition, the CD spectra of bLg AuNPs associated IAPP amyloids before and after X-ray irradiation were acquired.

Thioflavin T assay

IAPP fibrillization in the presence of the two types of AuNPs was analyzed by a thioflavin T (ThT) assay. The assay was performed under ambient conditions with 100 μL of total reaction volume per well, consisting of 25 μM ThT dye, 25 μM of IAPP and 0.083 mM or 0.11 mM of AuNPs in a 96 well-plate. The kinetic assay was carried out for 14 h with excitation and emission wavelengths of 440 nm and 485 nm at 25 °C. The kinetic parameters of lag time, fibrillation rate constant (k) and time to reach the half of fibrillization ($t_{1/2}$) were calculated from the ThT data.[16] The measurements were performed with 4 repeats for each sample condition and data was presented as mean ± standard deviation.

Atomic force microscopy

Aliquots of 20 μL of AuNP-IAPP solution (IAPP concentration: 25 μM, AuNPs: 0.083 mM, incubated 24 h) were deposited on freshly cleaved mica, left to adsorb for 2 min at room temperature, rinsed with MilliQ water, and gently dried with pressurized air. The samples were scanned on Nanoscope VIII Multimode Scanning Force Microscopes (Bruker) covered with an acoustic hood to minimize vibrational noise. The AFM was operated in tapping mode under ambient conditions using commercial silicon nitride cantilevers (Bruker). All AFM images were flattened to remove background curvature using the Nanoscope Analysis 1.5 software and no further image processing was carried out.

Cytotoxicity assay

The IAPP control and the AuNPs with IAPP were incubated with human embryonic kidney 293 (HEK293) cells or pancreatic βTC6 cells (acquired from ATCC) in DMEM supplemented with 15% FBS and 1% penicillin/streptomycin at 37 °C, 5% CO_2. Endpoint cytotoxicity was determined by the percentage of propidium iodide (PI) positive cells after 24 h. The experiment was performed in triplicate.

Dark-field imaging

bLg AuNPs-IAPP hybrids were incubated for 30 min with human plasma proteins or CEM.NKR-CCR5 human T cells, obtained from the Department of Microbiology and

Immunology, The Peter Doherty Institute for Infection and Immunity, The University of Melbourne. The samples were then mounted between a glass slide and a cover slip sandwiched with a double-sided tape and visualized by a dark-field microscope (CytoViva).

X ray-induced destruction of AuNP-IAPP hybrids

IAPP as well as bLg AuNPs-IAPP hybrids were irradiated with X rays using a Bruker D8 advanced X-ray generator. The X rays (Cu source, Type Gaussian) were generated at 125 W energy (25 kV and 5 mA) and directed to the center of the sample holder with an 8×8 μm slit. Samples were exposed for 100 s with a dose of 300 μSv/h. The exposed samples were immediately prepared for TEM after the X-ray treatment.

RESULTS & DISCUSSION

Synthesis and characterizations of bLg AuNPs and bLg-HDM AuNPs

Sonicated bLg fragments coated AuNPs via electrostatic interaction and surface adsorption, which prevented flocculation of the AuNPs against NaCl up to 2 M in concentration (Figure S1b, Supporting Information or SI). The AuNPs were monodisperse, but occasionally contained more than one NP per unit. The high stability of the bLg AuNPs (stable in water for at least 2 months of storage at 4 °C) is essential for their biological applications without evoking destabilization through ligand exchange.[11] The hydrolyzed bLg fragments were ~6 kDa.[17] The 1–2 nm thick 'coronas' of the bLg AuNPs (Figure 1a) were rich in β-sheets (>35%), resulting from bLg amyloids during the synthesis as corroborated by circular dichroism (CD) analysis (Figure 1e). In the CD spectra of bLg AuNPs, the negative peak absorbance around 218 nm indicates β-sheet conformation, whereas in the case of bLg-HDM AuNPs, the broad negative peak from 225 to 208 nm represents α-helices as the dominant conformation (Figure 1f). The presence of α-helices in the AuNPs could be due to heat-induced conversion of β-sheets.[18]

All-atom discrete molecular dynamics (DMD) simulations, a rapid and predictive molecular dynamics algorithm,[19, 20] were employed to provide a molecular insight into the corona formation of bLg fragments and denatured full-length bLg on the surface of AuNPs.[21] According to prior analysis of bLg amyloid formation and its binding with AuNPs,[9, 22] the amyloid-forming segment [117]LACQCL[122] from the native bLg sequence was chosen to model the AuNP-binding bLg amyloids, as described in the SI. The sequence is one of the most amyloidogenic regions in the native bLg sequence according to the zipperDB server, which estimates the propensity of a given 6- or 7-residue sequence in forming the steric zipper cross-β conformation,[18, 23] and contains two cysteines with strong binding affinity for AuNPs. We first evaluated the binding between a single sonicated bLg fibril (a two-layer β-sheet formed by ten peptides with the molecular mass of ~6 kDa as identified experimentally,[17] Figure S2) and a 4 nm spherical AuNP, where protein-AuNP interactions were adopted from the GolP force field (Methods, Figure S2b).[24] The cross-β fibrils bound the AuNP in two modes, with either the fibril interface being parallel or perpendicular to the AuNP surface (Figures S2d, e). With more cross-β fibrils added to the system, formation of fibril 'coronas' was observed due to strong fibril-AuNP binding and inter-fibril interactions on the AuNP surface (Figure 1c). The interaction between a heat-denatured bLg monomer

and an AuNP was also simulated at 350 K, where the unfolded protein was found to bind and spread over the AuNP surface with the native helices retained (Figure 1d, Figure S3), consistent with the CD measurement (Figures 1e, f).

Fibrillization of pathogenic IAPP in the presence of bLg AuNPs and bLg-HDM AuNPs

Upon incubation with IAPP monomers in the aqueous phase, bLg AuNPs appeared within the contours of the IAPP fibrils indicating intercalation of the NPs with the fibrils (Figure 2a). In contrast, bLg-HDM AuNPs, consisting of AuNPs stabilized by heat-denatured bLg monomers, protruded out of the fibril contours resulting from surface adsorption of the NPs onto the IAPP fibrils upon their incubation (Figure 2c). Ligand exchange between the protein coating of bLg AuNPs and free IAPP monomers (prior to fibrillization) was unfavorable, due to strong binding between bLg fragments and AuNPs, as reflected by the high stability of the NPs against salt (Figure S1b) and time. The association between the bLg AuNPs and IAPP fibrils was confirmed by energy-dispersive X-ray (EDX) mapping of the IAPP hybrids, which displayed a prominent elemental peak of Au (Figure S4). Three-dimensional atomic force microscopy (3D AFM) and AFM height scans (Figure 2e) further revealed intercalation (Figure 2b) or adsorption (Figure 2d) of AuNPs with respect to IAPP fibrils, consistent with the observations by transmission electron microscopy (TEM). It is necessary to mention that the IAPP fibrils alone were a mixture of different structural morphologies – many of the fibrils possessed the morphology of a twisted ribbon with a certain periodicity and handedness (Figures 2f, g), while the IAPP fibrils assembled in the presence of intercalated AuNPs did not display a distinct periodicity. This suggests a reduced cooperativity in the self-assembly of IAPP in the presence of the AuNPs.

The effects of the AuNPs on IAPP fibrillization were examined by a thioflavin T (ThT) kinetic assay (Figure 2h). The parameters of lag time, aggregation rate constant (k) and time to reach half of the fibrillization ($t_{1/2}$) were derived from the ThT data (Table S1).[16] As bLg AuNPs mostly intercalated with IAPP during fibrillization, they notably prolonged the lag time due to the inclusion of AuNPs in IAPP self-assembly. The intercalation observed for IAPP and bLg AuNPs at 0.083 mM (See reference 13 for calculation of AuNP concentration) was absent at 0.11 mM, as the NPs became adsorbed onto the fibril surfaces (Figure S5a). This can be understood as bLg AuNPs of high concentrations interacted more strongly among themselves, hence compromising NP-peptide interaction to favor peptide-peptide interaction.[5] However, such interaction was not observed for α-helix rich bLg-HDM AuNPs at all concentrations, indicating the intercalation of bLg AuNPs with IAPP was not merely kinetic driven, but through β-sheet stacking. Accordingly, the kinetic parameters for the case of bLg-HDM AuNPs resembled that of the IAPP control (Table S1). Time-dependent TEM imaging further revealed the dynamic processes of IAPP interacting with the AuNPs (Figure S6), where IAPP-AuNP binding and co-fibrillization started to occur within the first hour. In addition, both AuNPs were found adsorbed onto preformed IAPP fibrils (Figures S7a, b), suggesting that co-fibrillization occurred prior to the saturation phase. Moreover, the association between bLg AuNPs and amyloidogenic proteins was found to be independent from peptide sequence or charge, as it occurred for both cationic IAPP and anionic amyloid-β (1–42) (Figures S5b&c), further pointing to the role of β-sheet stacking in rendering the hybrid architectures.

To understand how bLg AuNPs were embedded within IAPP fibrils, docking simulations between model fibrils[25] of IAPP and bLg fragment were performed. Briefly, the β-sheets in two fibrils were pre-aligned in parallel or anti-parallel by shifting each residue, followed by DMD simulations for structural relaxation and binding energy estimation. The binding mode with the highest binding affinity was selected (Figure 3). The two segments of [8]ATQRLA[13] and [26]ILSSTN[31] facing each other in the IAPP amyloid fibril were found to bind the double-layered LACQCL fibril in parallel by extensive backbone hydrogen bonding as well as side-chain polar and hydrophobic interactions (Figure 3c). These two IAPP segments partially overlapped with the two amyloidogenic segments of IAPP, [13]ANFLVH[18] and [22]NFGAILS[28], whose amyloid structures belonged to the class 2 and class 7 steric zippers assuming a parallel, up-up, face-to-back and anti-parallel, up-up, face-to-back packing of β sheets, respectively.[23, 26] To confirm the fibrillization interactions of IAPP and bLg amyloids, we performed a ThT assay of IAPP in the presence of bLg amyloid seeds that were obtained by ultra-sonication of mature bLg amyloids (Figure S8). The enhanced ThT fluorescence and saturation plateau indicated the stimulatory effect of bLg amyloid seeds on IAPP fibrillization. Based on these observations and DMD simulations, we propose that IAPP fibrillization could be initiated by the existing bLg amyloid fragments on the AuNP surface, where the bLg fibrils had one of the fibril-growth interfaces bound to the 4-nm AuNP and the other one solvent-exposed and ready for co-fibrillization (Figure 3e).

Applications of co-fibrillization against amyloidogenesis

The two types of the AuNPs and the AuNP-IAPP hybrids were shown to be highly biocompatible with insulin-producing pancreatic βTC6 cells (Figure 2i) and human embryonic kidney (HEK293) cells (data not shown) and, most importantly, fully eliminated IAPP toxicity likely through sequestration of toxic IAPP oligomers and protofibrils with bLg. The AuNP-IAPP hybrids, with the coating of human plasma proteins (Figure 4a) to mimic the scenario of IAPP in circulation,[27] were clearly visible on dark-field microscopy via the surface plasmon resonance (SPR) of the AuNPs (CytoViva, Figure 4b). IAPP is synthesized and secreted by pancreatic islets for glycemic control, and has been found in the brain, heart and kidneys,[28, 29] in addition to their presence in circulation.[30] In the present study, phagocytosis of the hybrids by CEM.NKR-CCR5 human T cells was observed with dark-field microscopy (Figures 4c, d), circumventing the need of antibody labelling for immunogenic clearance of amyloid species in circulation.[31] Furthermore, X-ray irradiation of IAPP hybridized with bLg AuNPs induced potent destruction of the amyloid structures through localized heating of AuNPs (Figures 4e, f). Such effect was not observed for IAPP amyloids in the absence of AuNPs (Figure S9). It has been shown in the literature that X-ray irradiation of AuNPs resulted in localized hyperthermia (41~46 °C), which was exploited for targeted photo-thermal therapy of cancer without harming normal tissue.[32, 33] As the generated heat was highly confined to the bLg AuNPs embroidered inside IAPP fibrils, this scheme is not expected to induce significant damage to a cellular environment. The destructed IAPP fibrils were in the form of small aggregates. The β-sheet contents of IAPP-bLg AuNP hybrids were markedly reduced as a result of X-ray irradiation, from 34% to 5%, while the unordered contents were increased from 39% to 69% (Figures 4g, h), indicating that the destructed IAPP aggregates contained minimal toxic and β-sheet rich IAPP oligomers.[34]

bLg AuNPs prolonged the lag time to accommodate their intercalation within the IAPP fibrils. Such intercalation may be understood from the surfactant-like nature of amyloidogenic peptides, as the β-sheets of IAPP protofibrils/fibrils sought to minimize their exposure to the aqueous environment (and hence free energy) by interfacing the bLg β-sheets on the NP surfaces.[13] For bLg-HDM AuNPs, the lack of β-sheets (Figure 1e) coupled with their high zeta potential (Table S2) encouraged NP adsorption onto the IAPP fibrils. The short lag time (Figure 2h, Table S1) associated with bLg-HDM AuNPs may be attributed to heat-induced bLg denaturation and increased hydrophobicity, and hence increased affinity of bLg-HDM AuNPs for an IAPP 'halo' to facilitate fast fibrillization.[5]

CONCLUSION

Taken together, this study offers biomimetic AuNPs of coupling functional and pathogenic amyloids for toxicity elimination, X ray-induced destruction and dark-field imaging of phagocytosis of amyloid proteins, three new strategies for the detection and mitigation of amyloidogenesis associated with a number of human diseases.[31, 35] The novel synthesis schemes may be extended to the construction of other types of amyloid-metal biomimetics for biosensing. Furthermore, the molecular mechanism of β-sheet stacking between two amyloid species may have implications for understanding the *in vivo* cross-talk between proteins of different pathogenic origins that has so far eluded a biophysical underpinning.[36]

Supplementary Material

Refer to Web version on PubMed Central for supplementary material.

Acknowledgments

References

1. Ke PC, Sani MA, Ding F, Kakinen A, Javed I, Separovic F, Davis TP, Mezzenga R. Chem Soc Rev. 2017; 46:6492–6531. [PubMed: 28702523]

2. Knowles TP, Vendruscolo M, Dobson CM. Nat Rev Mol Cell Biol. 2014; 15:384–396. [PubMed: 24854788]

3. Maillet M, Van Berlo JH, Molkentin JD. Nat Rev Mol Cell Biol. 2013; 14:38–48. [PubMed: 23258295]

4. Moore KA, Pate KM, Soto-Ortega DD, Lohse S, van der Munnik N, Lim M, Jackson KS, Lyles VD, Jones L, Glassgow N. J Biol Eng. 2017; 11:5. [PubMed: 28191036]

5. Gladytz A, Abel B, Risselada HJ. Angew Chem Int Edit. 2016; 55:11242–11246.

6. Hamley IW, Kirkham S, Dehsorkhi A, Castelletto V, Adamcik J, Mezzenga R, Ruokolainen J, Mazzuca C, Gatto E, Venanzi M. Biomacromolecules. 2014; 15:3412–3420. [PubMed: 25105839]

7. Nyström G, Fernández-Ronco MP, Bolisetty S, Mazzotti M, Mezzenga R. Adv Mater. 2016; 28:393–393.

8. Bolisetty S, Boddupalli CS, Handschin S, Chaitanya K, Adamcik J, Saito Y, Manz MG, Mezzenga R. Biomacromolecules. 2014; 15:2793–2799. [PubMed: 24941321]

9. Bolisetty S, Mezzenga R. Nat Nanotech. 2016; 11:365–371.

10. Shen Y, Posavec L, Bolisetty S, Hilty FM, Nyström G, Kohlbrecher J, Hilbe M, Rossi A, Baumgartner J, Zimmermann MB, Mezzenga R. Nat Nanotech. 2017; 12:642–647.

11. Javed I, Hussain SZ, Shahzad A, Khan JM, Rehman M, Usman F, Razi MT, Shah MR, Hussain I. Colloid Surface B. 2016; 141:1–9.

12. Van de Broek B, Devoogdt N, D'Hollander A, Gijs HL, Jans K, Lagae L, Muyldermans S, Maes G, Borghs G. ACS Nano. 2011; 5:4319–4328. [PubMed: 21609027]

13. Jung JM, Savin G, Pouzot M, Schmitt C, Mezzenga R. Biomacromolecules. 2008; 9:2477–2486. [PubMed: 18698816]

14. Chanana M, Rivera_Gil P, Correa-Duarte MA, Liz-Marzán LM, Parak WJ. Angew Chem Int Edit. 2013; 52:4179–4183.

15. Whitmore L, Wallace BA. Biopolymers. 2008; 89:392–400. [PubMed: 17896349]

16. Cabaleiro-Lago C, Quinlan-Pluck F, Lynch I, Lindman S, Minogue AM, Thulin E, Walsh DM, Dawson KA, Linse S. J Am Chem Soc. 2008; 130:15437–15443. [PubMed: 18954050]

17. Lara C, Adamcik J, Jordens S, Mezzenga R. Biomacromolecules. 2011; 12:1868–1875. [PubMed: 21466236]

18. Narhi LO, Philo JS, Li T, Zhang M, Samal B, Arakawa T. Biochemistry. 1996; 35:11447–11453. [PubMed: 8784200]

19. Ding F, Tsao D, Nie H, Dokholyan NV. Structure. 2008; 16:1010–1018. [PubMed: 18611374]

20. Zhou Y, Karplus M. Nature. 1999; 401:400–403. [PubMed: 10517642]

21. Wang B, Seabrook SA, Nedumpully-Govindan P, Chen P, Yin H, Waddington L, Epa VC, Winkler DA, Kirby JK, Ding F. Phys Chem Chem Phys. 2015; 17:1728–1739. [PubMed: 25461673]

22. Akkermans C, Venema P, van der Goot AJ, Gruppen H, Bakx EJ, Boom RM, van der Linden E. Biomacromolecules. 2008; 9:1474–1479. [PubMed: 18416530]

23. Sawaya MR, Sambashivan S, Nelson R, Ivanova MI, Sievers SA, Apostol MI, Thompson MJ, Balbirnie M, Wiltzius JJ, McFarlane HT. Nature. 2007; 447:453. [PubMed: 17468747]

24. Hughes ZE, Wright LB, Walsh TR. Langmuir. 2013; 29:13217–13229. [PubMed: 24079907]

25. Luca S, Yau WM, Leapman R, Tycko R. Biochemistry. 2007; 46:13505–13522. [PubMed: 17979302]

26. Soriaga AB, Sangwan S, Macdonald R, Sawaya MR, Eisenberg D. J Phys Chem B. 2016; 120:5810–5816. [PubMed: 26629790]

27. Pilkington EH, Xing Y, Wang B, Kakinen A, Wang M, Davis TP, Ding F, Ke PC. Sci Rep. 2017; 7:2455. [PubMed: 28550295]

28. Gong W, Liu Z, Zeng C, Peng A, Chen H, Zhou H, Li L. Kidney Int. 2007; 72:213–218. [PubMed: 17495860]

29. Srodulski S, Sharma S, Bachstetter AB, Brelsfoard JM, Pascual C, Xie XS, Saatman KE, Van Eldik LJ, Despa F. Mol Neurodegener. 2014; 9:30. [PubMed: 25149184]

30. Despa S, Margulies KB, Chen L, Knowlton AA, Havel PJ, Taegtmeyer H, Bers DM, Despa F. Circ Res. 2012; 110:598–608. [PubMed: 22275486]

31. Richards DB, Cookson LM, Berges AC, Barton SV, Lane T, Ritter JM, Fontana M, Moon JC, Pinzani M, Gillmore JD. New Eng J Med. 2015; 373:1106–1114. [PubMed: 26176329]

32. Chatterjee DK, Diagaradjane P, Krishnan S. Ther Deliv. 2011; 2:1001–1014. [PubMed: 22506095]

33. Jain S, Hirst D, O'sullivan J. Brit J Radiol. 2012; 85:101–113. [PubMed: 22010024]

34. Laganowsky A, Liu C, Sawaya MR, Whitelegge JP, Park J, Zhao M, Pensalfini A, Soriaga AB, Landau M, Teng PK. Science. 2012; 335:1228–1231. [PubMed: 22403391]

35. Masters SL, Dunne A, Subramanian SL, Hull RL, Tannahill GM, Sharp FA, Becker C, Franchi L, Yoshihara E, Chen Z. Nat Immunol. 2010; 11:897–904. [PubMed: 20835230]

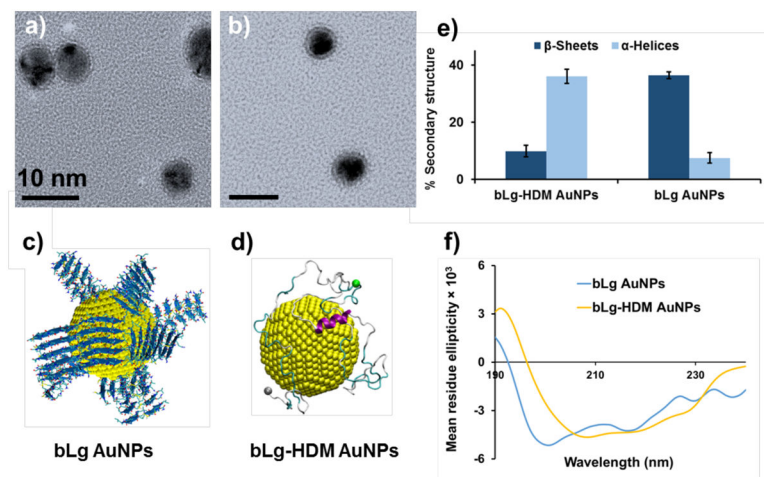36. Jackson K, Barisone GA, Diaz E, Jin Lw, DeCarli C, Despa F. Ann Neurol. 2013; 74:517–526. [PubMed: 23794448]

Figure 1.
Transmission electron microscopy (a, b) and discrete molecular simulations (c, d) show bLg AuNPs and bLg-HDM AuNPs. Circular dichroism spectroscopy indicates high β-sheet content in bLg AuNPs but not in bLg-HDM AuNPs (e, f). Scale bars in a, b: 10 nm. bLg amyloids of LACQCL (blue) coated on AuNPs (yellow spheres, 4 nm in diameter) (c). Full-length bLg molecules bound to an AuNP in the denatured state (d). Alpha-helices: purple, beta-sheets: orange, turns: cyan, coils: grey. C_α atoms in N- and C-termini: grey and green beads (d).
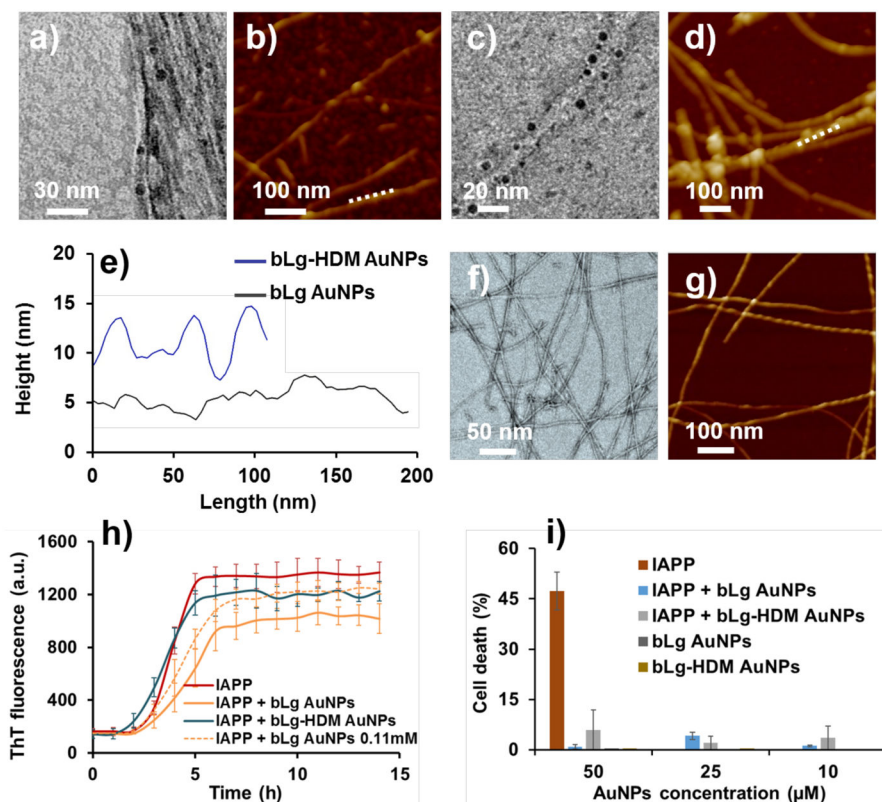
Figure 2.
Transmission electron microscopy (a, c) and atomic force microscopy (b, d) show bLg AuNPs and bLg-HDM AuNPs incubated with IAPP after 24 h of co-fibrillization. The AFM height scans of the IAPP fibrils (e) correspond to panels b, d (white dashed lines). The height variations of the blue trace indicate adsorption of bLg-HDM AuNPs, while the relatively flat contour of the black trace suggests intercalation of bLg AuNPs with IAPP fibrils, in agreement with the TEM image in panel a. While transmission electron microscopy showed the electron densities of IAPP fibrils incubated with the AuNPs (dark spots, a, c), 3D atomic force microscopy revealed topologies of the IAPP fibrils in the presence of the AuNPs (b, d). The IAPP fibrils appeared intercalated with bLg AuNPs (a) while surface-adsorbed with bLg-HDM AuNPs (c). The IAPP control is shown in (f, g). The effects of the AuNPs on IAPP fibrillization were evaluated by a thioflavin T kinetic assay (h), where the IAPP control (25 μM) displayed standard sigmoidal kinetics while the AuNPs (0.083 mM, unless specified otherwise) affected the kinetics as also summarized in Table S1. The toxicity induced by IAPP (fixed at 25 μM) in pancreatic βTC6 cells was fully eliminated in the presence of the AuNPs at 10–50 μM (i).
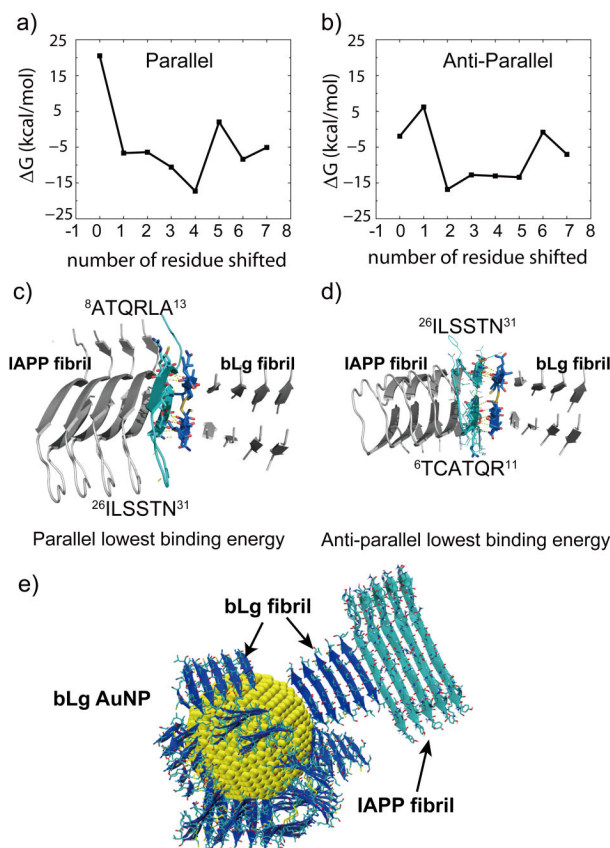
Figure 3.

Docking analysis between LACQCL and IAPP fibrils. The binding energy, ΔG, between the double-layered LACQCL and u-shaped IAPP fibrils, was plotted as a function of the number of shifted residues in parallel (a) and anti-parallel (b) alignments, respectively. The equilibrated snapshot structures with the corresponding lowest binding energies in parallel and anti-parallel are shown in (c, d). In both cases, similar regions in the IAPP bound to the LACQCL fibril, with the parallel alignment showing a slightly stronger binding affinity. A schematic of a bLg AuNP (4 nm) stacking with IAPP fibrils is illustrated in (e). bLg fibrils: blue. IAPP fibrils: cyan.
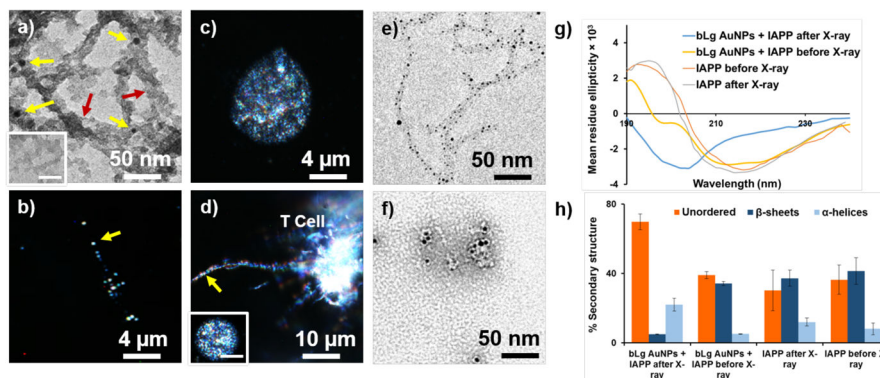
Figure 4.
Transmission electron microscopy and dark-field microscopy of bLg AuNP-IAPP hybrids coated with human plasma proteins (a, b: 24 h incubation; inset in a: plasma proteins without IAPP). Dark-field microscopy of human T cells (c) and human T cells phagocytosing a bLg AuNP-IAPP hybrid (d); inset in d: a T cell in the presence of IAPP fibrils. Scale bar: 4 µm. Yellow arrows: AuNPs. Red arrows: human plasma proteins. Destruction of IAPP amyloids via localized X-ray heating of bLg AuNPs before (e) and after (f) X-ray irradiation. CD spectra and corresponding secondary structures of IAPP control and IAPP hybridized with bLg AuNPs before and after X-ray irradiation (g, h).
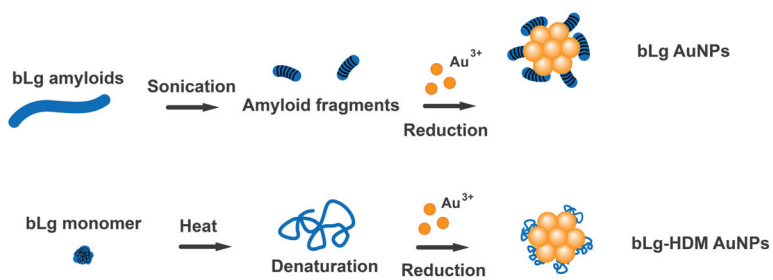
Scheme.

Synthesis of AuNPs stabilized by sonicated bLg amyloids (bLg AuNPs) and heat-denatured bLg monomers (bLg-HDM AuNPs).